

Antioxidation and DNA-binding properties of binuclear Er(III) complexes with Schiff-base ligands derived from 8-hydroxyquinoline-2-carboxaldehyde and four aroylhydrazines

Received August 27, 2009; accepted October 16, 2009; published online November 11, 2009

Yong-Chun Liu^{1,2} and Zheng-Yin Yang^{1,*}

¹College of Chemistry and Chemical Engineering, State Key Laboratory of Applied Organic Chemistry, Lanzhou University, Lanzhou 730000; and ²College of Chemistry and Chemical Engineering, Longdong University, Qingyang, Gansu 745000, P.R. China

*Zheng-Yin Yang, College of Chemistry and Chemical Engineering, State Key Laboratory of Applied Organic Chemistry, Lanzhou University, Lanzhou 730000, P.R. China, Tel: +86 931 891 3515, Fax: +86 931 891 2582, E-mail: yangzy@lzu.edu.cn

The Er(III) complexes are prepared from Er(NO₃)₃·6H₂O and Schiff-base ligands derived from 8-hydroxyquinoline-2-carboxaldehyde with four aroylhydrazines, including benzoylhydrazine, 2-hydroxybenzoylhydrazine, 4-hydroxybenzoylhydrazine and isonicotinylhydrazine, respectively. X-ray crystal and other structural analyses indicate that Er(III) and every ligand can form a binuclear Er(III) complex with nine-coordination and 1:1 metal-to-ligand stoichiometry at the Er(III) centre. All the Er(III) complexes can bind to calf thymus DNA through intercalation with the binding constants at the order of magnitude 10⁶ M⁻¹, and they may be used as potential anticancer drugs. All the Er(III) complexes have strong scavenging effects for hydroxyl radicals and superoxide radicals; however, complex containing active phenolic hydroxyl group shows stronger scavenging effects for hydroxyl radicals and complex containing *N*-heteroaromatic substituent shows stronger scavenging effects for superoxide radicals.

Keywords: Antioxidation/calf thymus DNA binding/rare earth/Schiff-base/X-ray crystallography.

Abbreviations: DNA, deoxyribonucleic acid; Tris, tris(hydroxymethyl)aminomethane; SD, standard deviation; DMSO, dimethyl sulfoxide; THF, tetrahydrofuran; TBP, TATA(-box)-binding protein.

Apart from the magnetic and photophysical properties, the bioactivities of lanthanides, such as antimicrobial, anti-tumour, antiviral, anticoagulant action, enhancing natural killer (NK) and macrophage cell activities, prevention from arteriosclerosis, etc., have been explored in recent decades (1–4). The chemistry of quinoline and its derivatives have also attracted special interest due to their therapeutic properties. Quinoline sulphonamides have been used in the

treatment of cancer, tuberculosis, diabetes, malaria and convulsion (5, 6). In addition, Schiff-bases are able to inhibit the growth of several animal tumours, and some metal chelates have shown good anti-tumour activities against animal tumours (7, 8). Therefore, well-designed organic ligands enable a fine-tuning of special properties of the metal ions. Previously, four Schiff-base ligands derived from 8-hydroxyquinoline-2-carboxaldehyde with aroylhydrazines, including benzoylhydrazine, 2-hydroxybenzoylhydrazine, 4-hydroxybenzoylhydrazine and isonicotinylhydrazine, were synthesized, and their Yb (III), Ho (III), Eu (III) and Nd (III) complexes were prepared, respectively, in our laboratory. We found that all these ligands and rare-earth metal complexes showed stronger antioxidation and DNA-binding properties (9–12). However, there were different structures and biological properties between these metal complexes. In this article, the Er(III) complexes were prepared from Er(NO₃)₃·6H₂O and the four Schiff-base ligands and their antioxidation and DNA-binding properties were investigated.

Materials and methods

Materials

Calf thymus DNA (CT-DNA) and ethidium bromide (EtBr) were obtained from Sigma–Aldrich Biotech. Co., Ltd 8-Hydroxyquinoline-2-carboxaldehyde was obtained from J&K Chemical Co., Ltd. All the stock solutions (1.0 mM) of the investigated complexes were prepared by dissolving the powder materials into appropriate amounts of dimethylformamide (DMF) solutions. Deionized double-distilled water and analytical grade reagents were used throughout. CT-DNA stock solution was prepared by dissolving the solid material in 5 mM Tris–HCl buffer (pH 7.20) containing 50 mM NaCl. The CT-DNA concentration in terms of base pair L⁻¹ was determined spectrophotometrically by employing an extinction coefficient of $\epsilon = 13,200 \text{ M}^{-1} \text{ cm}^{-1} (\text{base pair})^{-1}$ at 260 nm. The CT-DNA concentration in terms of nucleotide l⁻¹ was also determined spectrophotometrically by employing an extinction coefficient of $6,600 \text{ M}^{-1} \text{ cm}^{-1} (\text{nucleotide})^{-1}$ at 260 nm (13). EtBr was dissolved in 5 mM Tris–HCl buffer (pH 7.20) and its concentration was determined assuming a molar extinction coefficient of $5,600 \text{ l mol}^{-1} \text{ cm}^{-1}$ at 480 nm (14).

Instruments

Elemental analyses of C, N and H were carried out on an Elemental Vario EL analyzer. The metal ion content was determined by complexometric titration with EDTA after destruction of the complex in the conventional manner. The IR spectra were recorded on a Nicolet Nexus 670 FT-IR spectrometer using KBr disc in the 4000–400 cm⁻¹ region. ESI-MS (ESI-Trap/Mass) spectra were recorded on a Bruker Esquire 6000 Mass spectrophotometer. Ultraviolet-visible (UV–Vis) spectra were obtained using a PerkinElmer Lambda UV–Vis spectrophotometer.

Methods

Viscosity titration experiments were carried on an Ubbelohde viscometer in a thermostated water bath maintained at $25.00 \pm 0.01^\circ\text{C}$. Titrations were performed for an investigated compound that was introduced into DNA solution ($50 \mu\text{M}$, bps) present in the viscometer. Data were presented as $(\eta/\eta_0)^{1/3}$ versus the ratio of the compound to DNA, where η is the viscosity of DNA in the presence of the compound corrected from the solvent effect, and η_0 is the viscosity of DNA alone. Relative viscosities for DNA in either the presence or absence of compound were calculated from the following relation:

$$\eta = (t - t_0)/t_0 \quad (1)$$

where t is the observed flow time of the DNA containing solution, and t_0 is the flow time of buffer (14, 15).

Fluorescence spectra were recorded using RF-5301PC spectrofluorophotometer (Shimadzu, Japan) with a 1-cm quartz cell. Both of the excitation and emission bandwidths were 10 nm. All the experiments were measured after 5 min at a constant room temperature, 298 K. The intrinsic binding constants K_b could be obtained by the fluorescence titration methods and Scatchard equation (16):

$$r/C_f = n_b K_b - r K_b \quad (2)$$

where r is the moles of compound bound per mole nucleotides of DNA; C_f is the molar concentration of free compound; n_b is the number of binding sites or the maximum number of compound bound per nucleotide, and K_b is the association or binding constant. C_f and r could be calculated according to the following equations (17):

$$C_f = C_t - C_b \quad (3)$$

$$C_b = C_t(F - F_0)/(F_{\max} - F_0) \quad (4)$$

$$r = C_b/C_{\text{DNA}} \quad (5)$$

where C_t is the total molar concentration of compound; C_b is the molar concentration of compound bound for DNA; F is the observed fluorescence emission intensity at a given DNA concentration C_{DNA} (nucleotides); F_0 is the fluorescence emission intensity in the absence of DNA; and F_{\max} is the maximum fluorescence emission intensity of the compound totally bound for DNA at a titration end point. The binding constants were also obtained by McGhee and von Hippel model (18, 19):

$$\frac{r}{C_f} = K_b(1 - nr) \left[\frac{1 - nr}{1 - (n-1)r} \right]^{n-1} \quad (6)$$

where K_b is the intrinsic binding constant and n is the exclusion parameter in DNA base pairs. The experimental parameters K_b and n were adjusted to produce curves that gave, by inspection, the most satisfactory fits to the experimental data.

EtBr-DNA quenching assay was performed as reported in a literature but with small changes (20). DNA ($4.0 \mu\text{M}$, nucleotides) solution was added incrementally to $0.32 \mu\text{M}$ EtBr solution, until the rise in the fluorescence ($\lambda_{\text{ex}} = 496 \text{ nm}$, $\lambda_{\text{em}} = 596 \text{ nm}$) attained a saturation. Then, small aliquots of concentrated compound solutions (1.0 mM) were added till the drop in fluorescence intensity ($\lambda_{\text{ex}} = 525 \text{ nm}$, $\lambda_{\text{em}} = 587 \text{ nm}$) reached a constant value. Measurements were made after 5 min at a constant room temperature, 298 K. Stern–Volmer equation was used to determine the fluorescent quenching mechanisms (14):

$$F_0/F = 1 + K_q \tau_0 [Q] = 1 + K_{SV} [Q] \quad (7)$$

where F_0 and F are the fluorescence intensity in the absence and in the presence of a compound at $[Q]$ concentration, respectively; K_{SV} is the Stern–Volmer dynamic quenching constant; K_q is the quenching rate constant of bimolecular diffusion collision; τ_0 is the lifetime of free EtBr.

The hydroxyl radicals in aqueous media were generated through the Fenton-type reaction (21, 22). The 5-ml reaction mixtures contained 2.0 ml of 100-mM phosphate buffer (pH = 7.4), 1.0 ml of 0.10-mM aqueous safranin, 1 ml of 1.0-mM aqueous EDTA–Fe(II), 1 ml of 3% aqueous H_2O_2 and a series of quantitatively microadding solutions of the tested compound. The sample without the tested compound was used as the control. The reaction mixtures were incubated at 37°C for 60 min in a water bath. Absorbance at 520 nm was measured and the solvent effect was corrected throughout. The scavenging effect for OH^\cdot was calculated from the following expression (17, 23):

$$\text{Scavenging effect (\%)} = \frac{A_{\text{sample}} - A_{\text{blank}}}{A_{\text{control}} - A_{\text{blank}}} \times 100 \quad (8)$$

where A_{sample} is the absorbance of the sample in the presence of the tested compound, A_{blank} is the absorbance of the blank in the absence of the tested compound and A_{control} is the absorbance in the absence of the tested compound and EDTA–Fe(II).

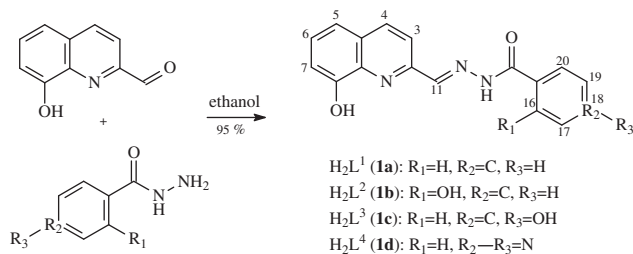
The superoxide radicals (O_2^\cdot) were produced by the MET–VitB₂–NBT system (17, 23). The solution of methionine (MET), vitamin B₂ (VitB₂) and nitroblue tetrazolium (NBT) were prepared with deionized double-distilled water under lightproof conditions, respectively. The 5-ml reaction mixtures contained 2.5 ml of 100-mM phosphate buffer (pH 7.8), 1.0 ml of 50-mM MET, 1.0 ml of 0.23-mM NBT, 0.50 ml of $33\text{-}\mu\text{M}$ VitB₂ and a series of quantitatively microadding solutions of the tested compound. After incubation at 30°C for 10 min in a water bath and then illuminated with a fluorescent lamp (4,000 Lux), the absorbance of the sample was measured at 560 nm and the solvent effect was corrected throughout. The sample reaction mixtures without the tested compound were used as the control. The scavenging effect for O_2^\cdot was calculated from the following expression:

$$\text{Scavenging effect (\%)} = \frac{A_0 - A_i}{A_0} \times 100 \quad (9)$$

where A_i is the absorbance in the presence of the tested compound, A_0 is the absorbance in the absence of the tested compound. The data for antioxidation presented as means \pm SD of three determinations and followed by Student's *t*-test. Differences were considered to be statistically significant if $p < 0.05$. IC_{50} value was introduced to denote the molar concentration of the tested compound which caused a 50% inhibitory or scavenging effect on hydroxyl radicals or superoxide radicals.

Syntheses of ligands

Four Schiff-base ligands, 8-hydroxyquinoline-2-carboxaldehyde-(benzoyl)hydrazone (H_2L^1 , **1a**), 8-hydroxyquinoline-2-carboxaldehyde-(2'-hydroxybenzoyl)hydrazone (H_2L^2 , **1b**), 8-hydroxyquinoline-2-carboxaldehyde-(4'-hydroxybenzoyl)hydrazone (H_2L^3 , **1c**) and 8-hydroxyquinoline-2-carboxaldehyde-(isoni-



Scheme 1 The synthetic routes for ligands (1a–d).

cotinyl)hydrazone (H_2L^4 , **1d**), were prepared from equimolar amounts of 8-hydroxyquinoline-2-carboxaldehyde and benzoylhydrazine, 2'-hydroxybenzoylhydrazine, 4'-hydroxybenzoylhydrazine and isonicotinylhydrazine, respectively (9–12). The synthetic routes for ligands are presented in Scheme 1.

Syntheses of metal complexes (2a–d)

Complex **2a** was prepared by refluxing and stirring equimolar amounts of a 40-ml methanol solution of ligand **1a** (0.058 g, 0.2 mM) and $Er(NO_3)_6 \cdot 6H_2O$ on a water bath. After refluxing for 30 min, triethylamine (0.020 g, 0.2 mM) was added into the reaction mixtures dropwise to deprotonate the phenolic hydroxyl substituent of 8-hydroxyquinolinato unit. Then, the mixtures were refluxed and stirred continuously for 8 h. After cooling to room temperature, the precipitate was centrifugalized, washed with methanol and dried in vacuum over 48 h to give an orange powder, yield 81.3% (0.090 g). Found: C 36.83, H 2.69, N 10.12, Er 30.13. Calcd for $C_{34}H_{30}N_8O_{14}Er_2$: C 36.78, H 2.70, N 10.10, Er 30.16. ESI-MS m/z 1,330.2 $[M+H]^+$ (DMF solution). IR (KBr): 3,382, 1,609, 1,552, 1,493, 1,310, 1,105, 1,030, 945, 811, 740, 658, 566, 493 cm^{-1} . UV–Vis (DMF/ H_2O): λ_{max} (ϵ) = 326 (44,700), 372 nm (33,900 $M^{-1} cm^{-1}$). Δm (DMF) = 40.2 $cm^2 \Omega^{-1} mol^{-1}$.

In the same way as **2a**, complexes **2b–d** were prepared from equimolar amounts of $Er(NO_3)_6 \cdot 6H_2O$ with **1b**, **1c** and **1d**, respectively:

- (i) Complex **2b**. Yield: 85.8%. Found: C 35.82, H 2.64, N 9.84, Er 29.37. Calcd for $C_{34}H_{30}N_8O_{16}Er_2$: C 35.75, H 2.63, N 9.81, Er 29.31. ESI-MS m/z 1,362.2 $[M+H]^+$ (DMF solution). IR (KBr): (cm^{-1}): 3,376, 3,193, 1,601, 1,570, 1,497, 1,310, 1,270, 1,103, 1,030, 930, 812, 756, 648, 575, 494. UV–Vis (DMF/ H_2O): λ_{max} (ϵ) = 330 (38,400), 376 nm (39,200 $M^{-1} cm^{-1}$). Δm (DMF) = 39.2 $cm^2 \Omega^{-1} mol^{-1}$.
- (ii) Complex **2c**. Yield: 90.8%. Found: C 35.79, H 2.63, N 9.83, Er 29.35. Calcd for $C_{34}H_{30}N_8O_{16}Er_2$: C 35.75, H 2.63, N 9.81, Er 29.31. ESI-MS m/z 1,362.2 $[M+H]^+$ (DMF solution). IR (KBr): (cm^{-1}): 3,392, 3,178, 1,599, 1,544, 1,489, 1,311, 1,290, 1,106, 1,055, 933, 804, 742, 637, 559, 490. UV–Vis (DMF/ H_2O): λ_{max} (ϵ) = 336 (45,400), 376 nm (39,400 $M^{-1} cm^{-1}$). Δm (DMF) = 39.3 $cm^2 \Omega^{-1} mol^{-1}$.
- (iii) Complex **2d**. Yield: 83.8%. Found: C 34.72, H 2.52, N 12.60, Er 29.96. Calcd for $C_{32}H_{28}N_{10}O_{14}Er_2$: C 34.56, H 2.52, N 12.60, Er 30.11. ESI-MS m/z 1,332.2 $[M+H]^+$ (DMF solution). IR (KBr): (cm^{-1}): 3,369, 1,636, 1,593, 1,550, 1,489, 1,314, 1,102, 1,059, 935, 814, 753, 612, 568, 492. UV–Vis (DMF/ H_2O): λ_{max} (ϵ) = 327 (44,300), 372 nm (36,500 $M^{-1} cm^{-1}$). Δm (DMF) = 43.4 $cm^2 \Omega^{-1} mol^{-1}$.

X-ray structure determination

The orange transparent, X-ray quality crystal of complex **2b** was obtained by vapour diffusion of diethyl ether into DMF solution of the powdered complex at room temperature for 2 weeks. X-ray diffraction data for a crystal were performed with graphite-monochromated Mo $K\alpha$ radiation (0.71,073 Å) on a Bruker APEX area-detector diffractometer and collected by the ω – 2θ scan technique at 296(2) K. The crystal structure was solved by direct methods. All non-hydrogen atoms were refined anisotropically by full-matrix least-squares methods on F^2 . A partial structure was obtained by direct methods and the remaining non-hydrogen atoms were located from difference maps. Hydrogen atoms were located in geometrically defined positions and not refined. All calculations were performed using the programs SHELXS-97 and SHELXL-97 (24). Crystal data and structure refinements for the X-ray structural analyses are presented in Table 1. Selected bond lengths and angles of the metal complex are presented in Supplementary Table S1.

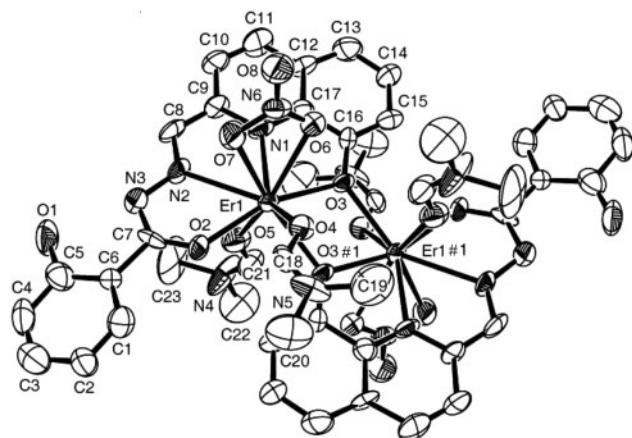
Results and discussion

Crystal structure analyses of complex 2b

The complex, formula $C_{46}H_{50}N_{12}O_{16}Er_2$, crystallizes with a dimension of $0.25 \times 0.23 \times 0.21 mm^3$ in the monoclinic system, space group $P2_1/c$, with lattice

Table 1. Crystal data and structure refinement of **2b** complex.

Complex	[ErL ² (NO ₃)(DMF) ₂] ₂
CCDC deposition number	715979
Chemical formula	C ₄₆ H ₅₀ N ₁₂ O ₁₆ Er ₂
Formula weight	1361.50
Crystal colour	orange
Temperature/K	296(2)
$\lambda/\text{\AA}$	Mo K α (0.71073)
Crystal system	Monoclinic
Space group	<i>P</i> 2 ₁ / <i>c</i>
<i>a</i> / \AA	11.684(3)
<i>b</i> / \AA	18.098(5)
<i>c</i> / \AA	12.778(4)
$\alpha/^\circ$	90.000
$\beta/^\circ$	95.341(4)
$\gamma/^\circ$	90.000
<i>V</i> / \AA^3	2,690.4(12)
<i>Z</i>	2
<i>D</i> _{calcd} /g cm ⁻³	1.681
<i>F</i> (000)	1348
μ/mm^{-1}	3.175
$\theta_{\text{min/max}}/^\circ$	1.75–22.14
Crystal dimension/mm ³	0.25 × 0.23 × 0.21
Reflections collected	9626
Independent reflections	3337 (<i>R</i> _{int} = 0.0551)
Index ranges	–12 ≤ <i>h</i> ≤ 11, –19 ≤ <i>k</i> ≤ 19, –13 ≤ <i>l</i> ≤ 9
Absorption correction	Semi-empirical from equivalents
Max. and min. transmission	0.456 and 0.514
Refinement method	Full-matrix least-squares on <i>F</i> ²
Data/restraints/parameters	3337/0/348
Goodness-of-fit on <i>F</i> ²	1.051
Final <i>R</i> indices [<i>I</i> > 2 σ (<i>I</i>)]	<i>R</i> ₁ = 0.0692, <i>wR</i> ₂ = 0.1651
<i>R</i> indices (all data)	<i>R</i> ₁ = 0.0865, <i>wR</i> ₂ = 0.1775
$\rho_{\text{min/max}}/\text{e}\text{\AA}^{-3}$	2.036/–1.474

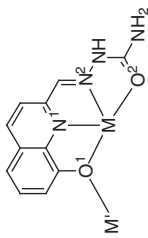
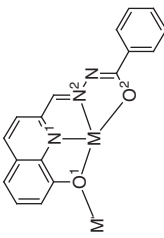
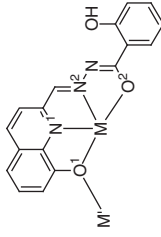
Fig. 1 The ORTEP diagram of [ErL²(NO₃)(DMF)₂]₂ complex.

parameters $a = 11.684(3) \text{ \AA}$, $b = 18.098(5) \text{ \AA}$, $c = 12.778(4) \text{ \AA}$, $\alpha = 90.00^\circ$, $\beta = 95.341(4)^\circ$, $\gamma = 90.00^\circ$, $F(000) = 1,348$, $\text{GOF} = 1.051$, $R_1 = 0.0692$, $wR_2 = 0.1651$, $Z = 2$. $D_{\text{calcd}} = 1.681 \text{ g cm}^{-3}$, $V = 2,690.4(12) \text{ \AA}^3$. The ORTEP diagram (30% probability ellipsoids) in Fig. 1 shows that the complex composition is of [ErL²(NO₃)(DMF)₂]₂. Ligand **1b** acts as a dibasic tetradentate ligand, binding to Er(III) through the phenolate oxygen atom, nitrogen atom of quinolinato

unit and the C=N group, [–]O–C=N– group (enolized and deprotonated from O=C–NH–) of the 2-hydroxybenzoylhydrazine side chain. In addition, one DMF molecule is binding orthogonally to the ligand-plane from one side to the metal ion, while another DMF and nitrate (bidentate) are binding from the other. Dimerization of this monomeric unit occurs through the phenolate oxygen atoms leading to a central planar four-membered (ErO)₂ ring with a Er···Er separation of 4.003 Å. At the dimerization site, a ‘set off’ of the two parallel ‘ErL²-planes’ by 1.615 Å takes place. On the basis of two molecules per unit cell, the density is calculated to be 1.681 g cm⁻³. The space group *P*2₁/*c* has four asymmetric units; therefore, the dimeric molecules need to be located on a centre of symmetry. The coordinate shows the centre of symmetry to be at 1/2, 1/2, 0. Thus the central four-membered (ErO)₂ ring is planar and the planes through the two ligands (**1b**) are parallel (1.615 Å). The bonded DMF molecule and the bonded nitrate are thus also related by a centre of symmetry to the respective moieties in the other half of the dimeric molecule. On the other hand, the 2-hydroxyl substituent linking with benzoylhydrazine does not take part in binding to Er(III), largely due to the steric effect and long distance between the 2-hydroxyl substituent and Er(III) (5.214 Å), but it may form an intramolecular hydrogen band with adjacent nitrogen atom (1.878 Å) of the same side chain.

This crystal structure of binuclear [ErL²(NO₃)(DMF)₂]₂ complex with nine-coordination and 1:1 metal-to-ligand stoichiometry is similar to that of [LaL(NO₃)(MeOH)₂]₂(NO₃)₂ complex, where ligand L-H is 2-[(8-hydroxyquinolinyl)methylene]hydrazine-carboxamide and acts as a tetradentate ligand binding to lanthanum(III) through the phenolate oxygen atom, nitrogen atom of quinolinato unit and the C=N group, C–O group of the semicarbazone side chain (2). The comparison of the structural parameters between them is shown in Table 2. First, O=C–NH– group of the 2-hydroxybenzoylhydrazine side chain has enolized and deprotonated into [–]O–C=N– group after the formation of [ErL²(NO₃)(DMF)₂]₂ complex, where the C–O bond length is 1.28(2) Å and the N–C double bond length is 1.30(2) Å. On the other hand, carbonyl group C=O of the semicarbazone side chain has not enolized in [LaL(NO₃)(MeOH)₂]₂(NO₃)₂. The difference in the deprotonation and enolization may well be due to the fact that triethylamine was added into the reaction mixtures to deprotonate the phenolic hydroxyl substituent of 8-hydroxyquinolinato unit during the formation of the Er(III) complex. However, carbonyl group C=O directly linking with aromatic group may be favourable for enolizing under the present experimental conditions than the non-aromatic group, such as –NH₂, when binding to metal ion and forming a complex. It is the enolization and deprotonation of O=C–NH– group changing into [–]O–C=N– that the [ErL²(NO₃)(DMF)₂]₂ complex is of neutral charge, but [LaL(NO₃)(MeOH)₂]₂(NO₃)₂ is an electrolyte. The enolization and deprotonation will afford an efficient route for investigators to design favourable

Table 2. Comparison of the structural parameters of ligand L-H⁽²⁾, 1a (H₂L¹) and 1b (H₂L²) when binding to different metal centres.

				
	[LaL(NO ₃ (MeOH)) ₂ (NO ₃) ₂]	[NdL ¹ (NO ₃ (DMF)) ₂]	[HoL ¹ (NO ₃ (DMF)) ₂]	[EuL ² (NO ₃ (DMF)) ₂]
O1-M	2.425(3)	2.4840(13)	2.4072(18)	2.430(4)
N1-M	2.541(3)	2.5538(16)	2.464(2)	2.513(5)
N2-M	2.620(4)	2.6087(15)	2.526(2)	2.583(5)
O2-M	2.414(3)	2.4165(13)	2.312(2)	2.331(12)
O1-M'	2.387(3)	2.4269(13)	2.3729(17)	2.421(4)
O1-M-N1	65.5(1)	64.06(4)	66.07(7)	66.3(4)
N1-M-N2	60.4(1)	61.66(5)	62.64(8)	62.6(5)
N2-M-O2	60.9(1)	60.67(5)	62.52(8)	62.8(5)
Parallel ML-planes	1.388	1.540	1.615	1.615
M M'	3.980	4.0356(7)	3.990	4.003
				[YbL ² (NO ₃ (DMF)) ₂ (DMF)]
				2.315(2)
				2.393(3)
				2.452(3)
				2.244(2)
				2.281(2)
				68.10(9)
				64.39(9)
				64.62(9)
				1.258
				3.7238(4)

molecules well. Second, the 'set off' of the two parallel 'ErL²-planes' by 1.615 Å takes place while the 'set off' of the two parallel 'LaL-planes' by accurately 1.388 Å (CCDC 273600) does, although they were reported by ~2 Å. The distance between the two parallel ML-planes and the distance between M...M' may result from the size of M³⁺ and substituent effects simultaneously.

In addition, this binuclear crystal structure of [ErL²(NO₃(DMF))₂]₂ complex with nine-coordination is much similar to those of [NdL¹(NO₃(DMF))₂]₂, [HoL¹(NO₃(DMF))₂]₂ and [EuL²(NO₃(DMF))₂]₂ complexes, but slightly different from binuclear [YbL²(NO₃(DMF))₂(DMF)] complex with eight-coordination (9-12), which may be related to the small size of Yb³⁺. Moreover, the typical bond lengths, the distances of parallel ML-planes and M...M' decrease by degrees with the decreasing of the size of Ln³⁺ for complexes formed from the same ligand as shown in Table 2.

Structural analysis for powdered complexes

Elemental analysis and molar conductance. All the powdered Er(III) complexes are of orange powders, stable in air and soluble in DMF and DMSO, but slightly soluble in methanol, ethanol, acetonitrile, ethyl acetate and acetone, THF and CHCl₃. The melting points of all the Er(III) complexes exceed 300°C. Elemental analyses indicate that all the Er(III) complexes are of 1:1 metal-to-ligand stoichiometry complexes, and the data of molar conductance of the Er(III) complexes in DMF solutions indicate that all of them act as non-electrolytes (25).

Infrared spectrum study of powdered complexes. Carefully compared with the characteristic IR bands of ligands, it comes to the conclusion that: (i) All the complexes show 3,392–3,369_{br} assigned to ν(OH) of H₂O; 945–930_w assigned to ρ_r (H₂O) and 658–612_w assigned to ρ_w (H₂O), indicating that there are coordinated water molecules participating in the Er(III) complexes (26, 27). (ii) All the complexes show 1,106–1,102 assigned to ν(C–OM), indicating that the binding of metal ion to every ligand through an O–M linkage takes place (28). (iii) 3,318–3,139_s assigned to ν(OH) and 1,288–1,267 assigned to ν(C–OH) of the phenolic hydroxyl substituent of ligands have disappeared, but the new bands of 3,193_s and 1,272_s can be respectively assigned to ν(OH) and ν(C–OH) of the phenolic hydroxyl substituent of 2-hydroxybenzoylhydrazine side chain of **2b** complex, while the new bands of 3,178_s and 1,290_s can also be respectively assigned to ν(OH) and ν(C–OH) of the phenolic hydroxyl substituent of 4-hydroxybenzoylhydrazine side chain of **2c** complex. (iv) 1,682–1,643_s assigned to ν(CO) and 3,576–3,320_{vs} assigned to ν(NH) of aroylhydrazine side chains of ligands have disappeared in all the IR spectra of Er(III) complexes, indicating that they participate in the Er(III) complexes with the groups of O=C–NH– of aroylhydrazine side chains enolizing and deprotonating into [–]O–C=N– as proved by the above crystal structural analysis. (v) 1,636–1,599 assigned to ν(CN) of azomethines of the Er(III)

complexes have shifted by 33–6 cm⁻¹ in comparison with bands of ligands, indicating that the nitrogen atoms of azomethines participate in the complexes. (vi) 1,570–1,544 assigned to $\nu(\text{CN})$ of pyridines of the Er(III) complexes have shifted by 38–6 cm⁻¹ in comparison with bands of ligands, indicating that the nitrogen atoms of pyridines also participate in the complexes. However, the new band of 1,593 can be assigned to $\nu(\text{CN})$ of free pyridine of isonicotinylhydrazine side chain of **2d** complex. (vii) 575–559_w assigned to $\nu(\text{MO})$ and 494–490_w assigned to $\nu(\text{MN})$ of the Er(III) complexes further indicate that oxygen atoms and nitrogen atoms participate in Er(III) complexes. (viii) All the Er(III) complexes show 1,497–1,489 (ν_1), 1,314–1,310 (ν_4), 1,059–1,030 (ν_2), 814–804 (ν_3), 756–740 (ν_5) and $\Delta\nu(\nu_1-\nu_4) = 187\text{--}175\text{ cm}^{-1}$, indicating that nitrate ions bidentately participate in the Er(III) complexes (9–12).

In addition, the ESI-MS data show that the m/z ($[\text{M} + \text{H}]^+$, DMF solution) are 1,330.1, 1,362.2, 1,362.2 and 1,332.1 for **2a**, **2b**, **2c** and **2d** complexes, respectively, indicating that the four coordinated water molecules for every powder Er(III) complex can be replaced by four DMF molecules when dissolved in DMF solution. However, the results of elemental analyses, molar conductance, IR and ESI-MS data indicate that all the powder metal complexes are structurally similar to each other and their compositions are of $[\text{ErL}^{1-4}(\text{NO}_3)(\text{H}_2\text{O})_2]_2$.

DNA-binding properties

Viscosity titration measurements. Viscosity titration measurements were carried out to clarify the interaction modes between the investigated compounds and CT-DNA. Viscosity measurements are very sensitive to changes in the length of DNA, as viscosity is proportional to L^3 for rod-like DNA of length L . Intercalation involves the insertion of a planar molecule between DNA base pairs, which results in a decrease in the DNA helical twist and lengthening of the DNA; therefore, intercalators cause the unwinding and lengthening of DNA helix as base pairs become

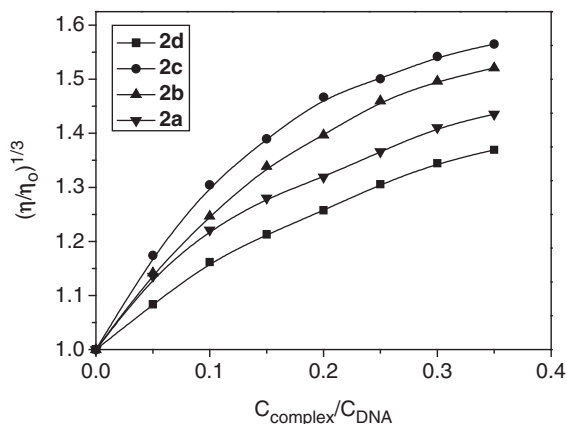


Fig. 2 Effects of increasing amounts of Er(III) complexes on the relative viscosity of CT-DNA in 5 mM Tris–HCl buffer solution (pH 7.20) containing 50 mM NaCl at 25.00 ± 0.01°C. The concentration of CT-DNA was 50 μM (bps).

separated to accommodate the binding compound (14, 29). On the other hand, agents bound to DNA through groove binding do not alter the relative viscosity of DNA, and agents electrostatically bound to DNA will bend or kink the DNA helix, reducing its effective length and its viscosity, concomitantly (15, 17). The effects of Er(III) complexes on the viscosities of CT-DNA are shown in Fig. 2. With the ratios of Er(III) complexes to DNA increasing, the relative viscosities of DNA increase steadily. This result indicates that there exist intercalations between all the Er(III) complexes with DNA helix, due to the fused multi-cyclic ring structures of Er(III) complexes which can unwind and lengthen the DNA helix (30).

UV–Vis spectroscopy study. The UV–Vis absorption spectra of the investigated compounds in the absence and in the presence of the CT-DNA were obtained in DMF:Tris–HCl buffer (5 mM, pH 7.20) containing 50 mM NaCl of 1:100 solutions, respectively. As shown in Supplementary Fig. S1, the UV–Vis spectra of Er(III) complexes have two types of absorption bands at λ_{max} in the regions of 326–336 nm ($\epsilon = 3.84\text{--}4.54 \times 10^4\text{ M}^{-1}\text{ cm}^{-1}$) and 372–376 nm ($\epsilon = 3.39\text{--}3.94 \times 10^4\text{ M}^{-1}\text{ cm}^{-1}$), which can be respectively assigned to $\pi\text{--}\pi^*$ transitions of the larger conjugated organic molecules and $\pi\text{--}\pi^*$ of the C=N–N=C groups coupled with charge transfers from ligands to metal ions ($\text{L} \rightarrow \text{Er}^{3+}$) (26, 27). Upon successive additions of CT-DNA, the UV–Vis absorption bands of Er(III) complexes **2a**, **2b** and **2c** show a progressive hypochromism of 28.6% at 326 nm, 28.8% at 330 nm and 39.7% at 336 nm by approximately saturated titration end points at $C_{\text{DNA}(\text{bps})}$: $C_{\text{complex}} = 1.2\text{--}1.8$: 1, respectively. Complexes **2a**, **2b** and **2c** show another progressive hypochromism of 27.9% at 372 nm, 28.7% at 376 nm and 39.3% at 376 nm, respectively. While complex **2d** show two types of slightly unsteady hypochromisms of 0.62% at 327 nm and 0.49% at 372 nm by an approximately saturated titration end point at $C_{\text{DNA}(\text{bps})}$: $C_{\text{complex}} = 1.4$: 1. There is no band shift for metal complexes apart from 2-nm red shifts for complex **2c**. In addition, isosbestic points at 407–415 nm are observed, indicating that the reaction between the investigated compound and DNA take place by an equilibrium. Absorption titration can monitor the interaction of a compound with DNA. The obvious hypochromism and red shift are usually characterized by the noncovalently intercalative binding of compound to DNA helix, due to the strong stacking interaction between the aromatic chromophore of the compound and base pairs of DNA (31, 32). However, the intercalation between a compound and DNA helix cannot be excluded only by no or small red shift of UV–Vis absorption bands. In fact, some groove binders of Hoechst 33, 258 family can also present red shifts or even blue shifts of absorption bands when they bind to DNA helix by groove binding modes, especially for multiple binders (33, 34). After all, hydrodynamic measurements that are sensitive to length change of DNA (*i.e.* viscosity and sedimentation) are regarded as the least ambiguous and the most critical criterions for

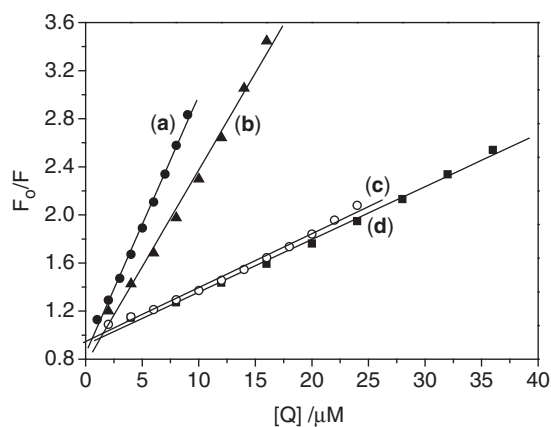


Fig. 3 Stern–Volmer plots of F_0/F versus $[Q]$ for Er(III) complexes. Tests were performed in the conditions of 5 mM Tris–HCl buffer containing 50 mM NaCl at 298 K. $C_{\text{DNA}} = 4 \mu\text{M}$ (nucleotides), $C_{\text{EtBr}} = 0.32 \mu\text{M}$; $\lambda_{\text{ex}} = 525 \text{ nm}$, $\lambda_{\text{em}} = 587 \text{ nm}$. Lines of (a), (b), (c) and (d) for complexes **2c**, **2b**, **2a** and **2d**, respectively.

binding modes in solution in absence of crystallographic structural data (35, 36).

On the other hand, the appreciable hypochromisms of Er(III) complexes intercalating to DNA present the order of **2c** > **2b** > **2a** > **2d**, which is in good agreement with the result of viscosity titration measurements. The appreciable hypochromisms are parallel to the intercalative strengths and the affinities of compounds binding to DNA (37). Here, the phenolic hydroxy groups that can bind to nucleotides or/and the sugar–phosphate backbone of DNA through hydrogen bonds may play key roles in the interactions for **2c** and **2b** complexes. As for complex **2d**, *N* atom of aromatic sextet of the pyridine ring of isonicotinylhydrazine side chain has an exposed and non-hybridized *p* orbital containing long pair electron, which may result in a stronger electronic repulsion and hinder the π – π stacking interaction. Moreover, the aggregation of self-stacked molecules of **2d** may occur, which will induce the possibility of an association/dissociation equilibrium in the absence of DNA, and induce a slightly unsteady UV–Vis absorption and a little hypochromism even in an excess of conjugate versus DNA-binding proteins (bps) (34). However, the order of the appreciable hypochromisms of Er(III) complexes are not in agreement with those of Yb (III), Ho (III), Eu (III) and Nd (III) complexes (9–12), which may result from the different metal centres.

EtBr–DNA quenching assay. The fluorescence emission intensity of DNA–EtBr system decreased dramatically upon the increasing amounts of every Er(III) complex. Stern–Volmer equation was used to determine the fluorescent quenching mechanism (14). Plots of F_0/F versus $[Q]$ are shown in Fig. 3 and the quenching data collected and calculated from the good linear relationship when $p < 0.05$ are listed in Table 3. As shown, the data of K_{SV} are 4.384 – $21.96 \times 10^4 \text{ M}^{-1}$, and the data of K_{q} calculated are 2.436 – $12.20 \times 10^{13} \text{ M}^{-1} \text{ s}^{-1}$ for Er(III) complexes, when the value of τ_0 is taken as $1.8 \times 10^{-9} \text{ s}$ (14).

Table 3. Parameters of K_{b} , K_{SV} , K_{q} , CF_{50} , IC_{50} (OH^- and O_2^-) for Er(III) complexes.

Compound	$K_{\text{b}} \times 10^6 \text{ M}^{-1}$	$1/n^a$	$K_{\text{SV}} \times 10^4 \text{ M}^{-1} (R)$	$K_{\text{q}} \times 10^{13} \text{ M}^{-1} \text{ s}^{-1}$	CF_{50}^b (μM) ($C_{\text{compound}}/C_{\text{DNA, nucleotides}}$)	$IC_{50}^c \pm \text{SD}$ (μM) for $\text{OH}^\bullet (R)$	$IC_{50}^c \pm \text{SD}$ (μM) for $\text{O}_2^- (R)$
2a	3.955 ± 0.898	0.15	4.479 ± 0.134 (0.9955)	2.488	23.48 (5.870)	13.75 ± 0.51 (0.9958)	8.362 ± 0.360 (0.9944)
2b	3.147 ± 0.979	0.28	16.10 ± 0.65 (0.9951)	8.944	7.665 (1.916)	6.998 ± 0.215 (0.9867)	10.20 ± 0.35 (0.9965)
2c	4.046 ± 1.163	0.22	21.96 ± 0.53 (0.9980)	12.20	5.120 (1.280)	3.122 ± 0.072 (0.9882)	14.01 ± 0.69 (0.9929)
2d	3.681 ± 0.758	0.36	4.384 ± 0.105 (0.9980)	2.436	24.65 (6.163)	19.85 ± 0.54 (0.9943)	6.026 ± 0.237 (0.9936)

^aThe data of $1/n$ represent moles of compound/mol of base pair of DNA. ^b CF_{50} represents the molar concentration of the tested compound that causes a 50% loss in the fluorescence intensity of EtBr–DNA system. ^c IC_{50} value was calculated from regression line of the log of the tested compound concentration versus the scavenging effect (%) of the compound. *R* represents the linear correlation coefficient.

All of the current values of K_q are much greater than that of $K_{q(\max)}$ ($2.0 \times 10^{10} \text{ M}^{-1} \text{ s}^{-1}$), the maximum quenching rate constant of bimolecular diffusion collision, which are indicative of static types of quenching mechanisms arisen from the formations of dark complexes between the fluorophores and quenching agents (38, 39). The loss of fluorescence intensity at the maximum wavelength indicates the displacement of EtBr from DNA–EtBr complex by a compound and the intercalative binding between the compound with DNA (17). The EtBr–DNA quenching results also indicate that most of the EtBr molecules have been displaced from EtBr–DNA complex by every quencher at the approximately saturated end point. Additionally, the Stern–Volmer dynamic quenching constants can also be interpreted as binding affinities of the complexation reactions (40, 41). The data of K_{SV} present the order of $2c > 2b > 2a > 2d$, which indicate the abilities of displacement of EtBr from EtBr–DNA systems by complexes and the binding affinities between complexes and DNA. However, the order is in good agreement with the UV–Vis spectroscopy study results.

More importantly, DNA intercalators have been used extensively as anti-tumour, antineoplastic, anti-malarial, antibiotic and antifungal agents (14). There is a criterion for screening out anti-tumour drugs from others by EtBr–DNA fluorescent tracer method, *i.e.* a compound can be used as potential anti-tumour drug if it causes a 50% loss of EtBr–DNA fluorescence intensity by fluorescent titrations before the molar concentration ratio of the compound to DNA (nucleotides) does not overrun 100:1 (42). CF_{50} value is introduced to denote the molar concentration of a compound that causes a 50% loss in the fluorescence intensity of EtBr–DNA system. According to the data of CF_{50} and the molar ratios of compounds to DNA shown in Table 3, it is interesting to note that at CF_{50} all the molar concentration ratios of the Er(III) complexes to DNA (1.280–16.58:1) are largely under 100:1, indicating that all these Er(III) complexes can be used as potential anti-tumour drugs. However, their pharmacodynamical, pharmacological and toxicological properties require further study *in vivo*.

Fluorescence spectroscopy study. When excited at $\lambda_{\text{ex}} = 324\text{--}331 \text{ nm}$ the Er(III) complexes showed the fluorescence maximum wavelengths at $\lambda_{\text{em}} = 406\text{--}423 \text{ nm}$. Upon additions of DNA, the fluorescence emission intensity of every investigated compound grew steadily. Although the emission enhancement cannot be regarded as a rigid criterion for binding mode, it is related to the extent to which the compound gets into a hydrophobic environment inside DNA and avoids the effect of solvent water molecules (17). Scatchard plot should be a straight line for a simple binding reaction. Because of the significant neighbour exclusion property of DNA binding to intercalating agents, the Scatchard plot of r/C_f versus r usually presents a deviation from linearity (18). As shown in Supplementary Fig. S2, every Scatchard plot of r/C_f versus r for Er(III) complexes show a deviation from linearity, so the binding constant was obtained by

the McGhee and von Hippel model (18, 19). The data of binding constants (K_b) and the moles of compound bound per mole of base pair of DNA ($1/n$) are shown in Table 3. In addition, the binding constant (K_b) of EtBr to CT-DNA studied as the same methods and the same conditions of the investigated complexes present the order of magnitude at $3.166 (\pm 0.145) \times 10^6 \text{ M}^{-1}$ ($1/n = 0.24$) as shown in Supplementary Fig. S2 (E, E'), which is consistent with the previous study result (EtBr–DNA, $K_b = 3.0 \times 10^6 \text{ M}^{-1}$ in 5 mM Tris–HCl/50 mM NaCl buffer, pH = 7.2). The data of binding constants (K_b) of complexes present $3.147\text{--}4.046 \times 10^6 \text{ M}^{-1}$, indicating that these Er(III) complexes can bind to DNA effectively (43).

Antioxidation

Hydroxyl radical and superoxide radical scavenging activities. Figure 4A show the plots of hydroxyl radical scavenging effect (%) for Er(III) complexes, which are concentration dependent. As shown in Table 3, the values of IC_{50} of Er(III) complexes for hydroxyl radical scavenging effect are $3.122\text{--}19.85 \mu\text{M}$ with the order of $2c < 2b < 2a < 2d$. This order of IC_{50} is opposite to the abilities of scavenging effects for hydroxyl radicals. It is marked that the hydroxyl radical scavenging effects of **2c** and **2b** are higher than those of **2a** and **2d**, possibly due to the key roles of functional

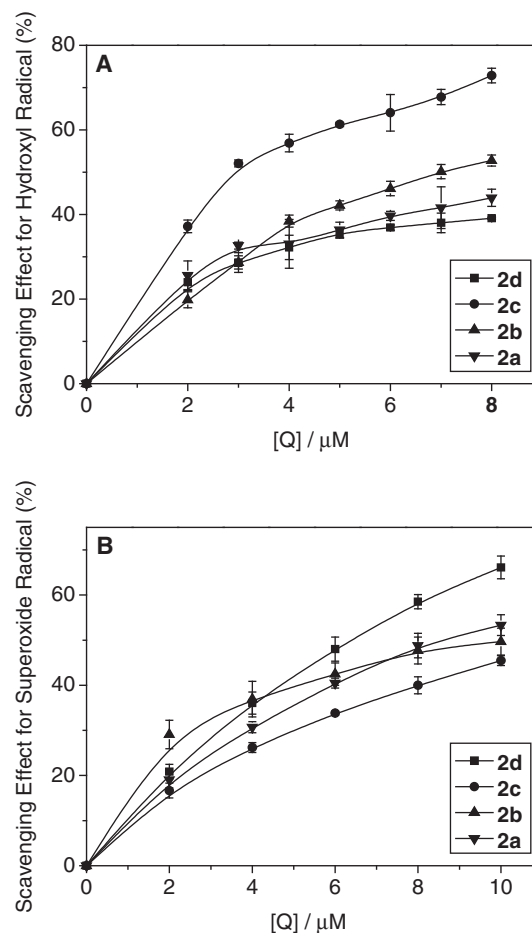


Fig. 4 Plots of antioxidation properties for Er(III) complexes. (A) and (B) represent the hydroxyl radical scavenging effect (%) and superoxide radical scavenging effect (%), respectively.

groups, $-\text{OH}$, which can react with HO^\bullet to form stable macromolecular radicals by the typical H-abstraction reaction (44). Figure 4B show the plots of superoxide radical scavenging effect (%) for Er(III) complexes, which are also concentration dependent. As shown in Table 3, the values of IC_{50} are 6.026–14.01 μM with the order of $2\text{d} < 2\text{a} < 2\text{b} < 2\text{c}$. This result suggests that complex containing *N*-heteroaromatic substituent shows stronger scavenging effect for superoxide radicals than others, and that there are different mechanisms between scavenging hydroxyl radicals and superoxide radicals.

It is reported that the value of IC_{50} of ascorbic acid (Vc), a standard agent for non-enzymatic reaction, for hydroxyl radicals is 1.537 mg ml^{-1} (8.727 mM), and the scavenging effect of Vc for superoxide radicals is only 25% at 1.75 mg ml^{-1} (9.94 mM) (45). It is pronounced that all the Er(III) complexes investigated here have much stronger scavenging abilities for hydroxyl radicals and superoxide radicals than ascorbic acid (Vc). Endowed with antioxidative properties, these DNA binders may be effective inhibitors of the formation of a DNA/TBP complex topoisomerases (46–48).

Comparative properties of ligands and complexes Yb (III), Er(III), Ho (III), Eu (III) and Nd (III)

Antioxidation and DNA-binding properties of ligands (1a–d) and Er(III) (2a–d), Nd (III) (3a–d), Eu (III) (4a–d), Ho (III) (5a–d) and Yb (III) (6a–d) complexes (9–12) are listed in Supplementary Table S2. It is found that all these complexes have stronger DNA-binding properties than ligands, and that complexes containing active phenolic hydroxyl groups have stronger DNA-binding properties than others. Particularly, complex 6c shows the strongest DNA-binding properties. However, all the complexes and ligands can be used as potential anticancer drugs but the anti-tumour activities of complexes may be better than that of ligands. It is also found that complexes containing active phenolic hydroxyl group have stronger scavenging effects for hydroxyl radicals but complexes containing *N*-heteroaromatic substituents show stronger scavenging effects for superoxide radicals than others. In particular, 5c and 3d complexes show the strongest scavenging effects for hydroxyl radicals and superoxide radicals, respectively.

Conclusion

The Er(III) complexes are prepared from $\text{Er}(\text{NO}_3)_3 \cdot 6\text{H}_2\text{O}$ and Schiff-base ligands derived from 8-hydroxyquinoline-2-carboxaldehyde with four aroylhydrazines. X-ray crystal and other structural analyses show that Er(III) and every ligand can form a binuclear Er(III) complex with nine-coordination and 1:1 metal-to-ligand stoichiometry at the Er(III) centre. Every ligand acts as a dibasic tetradentate ligand, binding to Er(III) through the phenolate oxygen atom, nitrogen atom of quinolinato unit and the $\text{C}=\text{N}$ group, $^-\text{O}-\text{C}=\text{N}-$ group (enolized and deprotonated from $\text{O}=\text{C}-\text{NH}-$ group) of the aroylhydrazine side chain. One DMF molecule is binding orthogonally to the ligand-plane from one side to the

metal ion, while another DMF and nitrate (bidentate) are binding from the other. Dimerization of this monomeric unit occurs through the phenolate oxygen atoms leading to a central four-membered $(\text{ErO})_2$ -ring. It is the key roles of enolization and deprotonation of $\text{O}=\text{C}-\text{NH}-$ group changing into $^-\text{O}-\text{C}=\text{N}-$ of the aroylhydrazine side chain that the dimeric centronucleus of every Er(III) complex is of neutral charge, which will afford an efficient route for investigators to well design favourable molecules. In addition, all the Er(III) complexes can bind to CT-DNA through intercalations with the binding constants at 10^6M^{-1} , but Er(III) complexes present stronger affinities to DNA than ligands. EtBr–DNA fluorescent tracer methods show that all these Er(III) complexes can be used as potential anticancer drugs but the anti-tumour activities of Er(III) complexes may be better than that of ligands. However, their pharmacodynamical, pharmacological and toxicological properties require further study *in vivo*.

On the other hand, all these Er(III) complexes have strong abilities of antioxidation for hydroxyl radicals and superoxide radicals. Er(III) complex containing active phenolic hydroxy groups presents stronger abilities of scavenging effects for hydroxyl radicals and Er(III) complex containing *N*-heteroaromatic substituent shows stronger scavenging effects for superoxide radicals than others. However, the complex 2c has lower ability of scavenging superoxide radicals and the different mechanisms between scavenging hydroxyl radicals and superoxide radicals require further study.

Supplementary data

Supplementary Data are available at *JB* Online.

Funding

The study was supported by the National Natural Science Foundation of China (20975046).

Conflict of interest

None declared.

References

- Parker, D., Dickins, R.S., Puschmann, H., Crossland, C., and Howard, J.A.K. (2002) Being excited by lanthanide coordination complexes: aqua species, chirality, excited-state chemistry, and exchange dynamics. *Chem. Rev.* **102**, 1977–2010
- Albrecht, M., Osetska, O., and Fröhlich, R. (2005) 2-[(8-Hydroxyquinolinyl)methylene]hydrazinecarboxamide: expanding the coordination sphere of 8-hydroxyquinoline for coordination of rare-earth metal (III) ions. *Dalton Trans.* **23**, 3757–3762
- Hunter, R.B. and Walker, W. (1956) Anticoagulant action of neodymium 3-sulpho-isonicotinate. *Nature* **178**, 47
- Kramsch, D.M., Aspen, A.J., and Rozler, L.J. (1981) Atherosclerosis: prevention by agents not affecting abnormal levels of blood lipids. *Science* **213**, 1511–1512
- Schmidt, L.H. (1969) Chemotherapy of the drug-resistant Malarías. *Ann. Rev. Microbiol.* **23**, 427–454

6. El-Asmy, A.A., El-Sonbati, A.Z., Ba-Issa, A.A., and Mounir, M. (1990) Synthesis and properties of 7-formyl-8-hydroxyquinoline and its transition metal complexes. *Transit. Metal Chem.* **5**, 222–225
7. Hodnett, E.M. and Mooney, P.D. (1970) Antitumor activities of some Schiff bases. *J. Med. Chem.* **13**, 786–786
8. Hodnett, E.M. and Dunn, W.J. (1972) Cobalt derivatives of Schiff bases of aliphatic amines as antitumor agents. *J. Med. Chem.* **15**, 339–339
9. Liu, Y.-C. and Yang, Z.-Y. (2009) Crystal structures, antioxidation and DNA binding properties of Yb(III) complexes with Schiff-base ligands derived from 8-hydroxyquinoline-2-carbaldehyde and four aroylhydrazines. *Biometals* **22**, 733–751
10. Liu, Y.-C. and Yang, Z.-Y. (2009) Synthesis, crystal structure, antioxidation and DNA binding properties of binuclear Ho(III) complexes of Schiff-base ligands derived from 8-hydroxyquinoline-2-carboxyaldehyde and four aroylhydrazines. *J. Organomet. Chem.* **694**, 3091–3101
11. Liu, Y.-C. and Yang, Z.-Y. (2009) Crystal structures, antioxidation and DNA binding properties of Eu(III) complexes with Schiff-base ligands derived from 8-hydroxyquinoline-2-carboxyaldehyde and three aroylhydrazines. *J. Inorg. Biochem.* **103**, 1014–1022
12. Liu, Y.-C. and Yang, Z.-Y. (2009) Antioxidation and DNA binding properties of binuclear Nd(III) complexes with Schiff-base ligands derived from 8-hydroxyquinoline-2-carboxyaldehyde and four aroylhydrazides. *Inorg. Chem. Commun.* **12**, 704–706
13. Zsila, F., Bikádi, Z., and Simonyi, M. (2004) Circular dichroism spectroscopic studies reveal pH dependent binding of curcumin in the minor groove of natural and synthetic nucleic acids. *Org. Biomol. Chem.* **2**, 2902–2910
14. Suh, D. and Chaires, J.B. (1995) Criteria for the mode of binding of DNA binding agents. *Bioorg. Med. Chem.* **3**, 723–728
15. Satyanarayana, S., Dabrowiak, J.C., and Chaires, J.B. (1992) Neither Δ -nor Δ -Tris(phenanthroline)ruthenium (II) Binds to DNA by Classical Intercalation. *Biochemistry* **31**, 9319–9324
16. Scatchard, G. (1949) The attractions of protein for small molecules and ions. *Ann. NY. Acad. Sci.* **51**, 660–673
17. Wang, B.D., Yang, Z.Y., Crewdson, P., and Wang, D.Q. (2007) Synthesis, crystal structure and DNA-binding studies of the Ln(III) complex with 6-hydroxychromone-3-carbaldehyde benzoyl hydrazone. *J. Inorg. Biochem.* **101**, 1492–1504
18. Chaires, J.B., Dattagupta, N., and Crothers, D.M. (1982) Studies on interaction of anthracycline antibiotics and deoxyribonucleic acid: equilibrium binding studies on the interaction of daunomycin with deoxyribonucleic acid. *Biochemistry* **21**, 3933–3940
19. McGhee, J.D. and von Hippel, P.H. (1974) Theoretical aspects of DNA–protein interactions: co-operative and non-co-operative binding of large ligands to a one-dimensional homogeneous lattice. *J. Mol. Biol.* **86**, 469–489
20. Krishna, A.G., Kumar, D.V., Khan, B.M., Rawal, S.K., and Ganesh, K.N. (1998) Taxol–DNA interactions: fluorescence and CD studies of DNA groove binding properties of taxol. *Biochimica et Biophysica Acta* **1381**, 104–112
21. Winterbourn, C.C. (1981) Hydroxyl radical production in body fluids. Roles of metal ions, ascorbate and superoxide. *Biochem. J.* **198**, 125–131
22. Winterbourn, C.C. (1979) Comparison of superoxide with other reducing agents in the biological production of hydroxyl radicals. *Biochem. J.* **182**, 625–628
23. Guo, Z.Y., Xing, R.E., Liu, S., Yu, H.H., Wang, P.B., Li, C.P., and Li, P.C. (2005) The synthesis and antioxidant activity of the Schiff bases of chitosan and carboxymethyl chitosan. *Bioorg. Med. Chem. Lett.* **15**, 4600–4603
24. Sheldrick, G.M. (1990) Phase annealing in SHELX-90: direct methods for larger structures. *Acta Crystallogr. A* **46**, 467–473
25. Geary, W.J. (1971) The use of conductivity measurements in organic solvents for the characterisation of coordination compounds. *Coord. Chem. Rev.* **7**, 81–122
26. Moawad, M.M. and Hanna, W.G. (2002) Structural and antimicrobial studies of some divalent transition metal complexes with some new symmetrical bis(7-formylanil substituted-sulfoxine) Schiff base ligands. *J. Coord. Chem.* **55**, 439–457
27. Ismail, T.M.A. (2005) Mononuclear and binuclear Co(II), Ni(II), Cu(II), Zn(II) and Cd(II) complexes of Schiff-base ligands derived from 7-formyl-8-hydroxyquinoline and diamionaphthalenes. *J. Coord. Chem.* **58**, 141–151
28. Ou-Yang, J.M. (1997) Synthesis properties and characterization of the complexes of 2-(N-hexadecylcarbamoyl)-8-hydroxyquinoline. *J. Inorg. Chem. (in Chinese)* **13**, 315–319
29. Palchadhuri, R. and Hergenrother, P.J. (2007) DNA as a target for anticancer compounds: methods to determine the mode of binding and the mechanism of action. *Curr. Opin. Biotechnol.* **18**, 497–503
30. Snyder, R.D. (2007) Assessment of atypical DNA intercalating agents in biological and in silico systems. *Mutat. Res.* **623**, 72–82
31. Barton, J.K., Danishefsky, A.T., and Goldberg, J.M. (1984) Tris(phenanthroline)ruthenium(II): stereoselectivity in binding to DNA. *J. Am. Chem. Soc.* **106**, 2172–2176
32. Lu, H.L., Liang, J.J., Zeng, Z.Z., Xi, P.X., Liu, X.H., Chen, F.J., and Xu, Z.H. (2007) Three salicylaldehyde derivative Schiff base Zn^{II} complexes: synthesis, DNA binding and hydroxyl radical scavenging capacity. *Transit. Metal Chem.* **32**, 564–569
33. Behrens, C., Harrit, N., and Nielsen, P.E. (2001) Synthesis of a Hoechst 33258 analogue amino acid building block for direct incorporation of a fluorescent, high-affinity DNA binding motif into peptides. *Bioconjugate Chem.* **12**, 1021–1027
34. Frau, S., Bernadou, J., and Meunier, B. (1997) Nuclease activity and binding characteristics of a cationic “manganese porphyrin-Bis(benzimidazole) dye (Hoechst 33258)” conjugate. *Bioconjugate Chem.* **8**, 222–231
35. Sigman, D.S., Mazumder, A., and Perrin, D.M. (1993) Chemical nucleases. *Chem. Rev.* **93**, 2295–2316
36. Wang, Y., Yang, Z.Y., Wang, Q., Cai, Q.K., and Yu, K.B. (2005) Crystal structure, antitumor activities and DNA-binding properties of the La(III) complex with Phthalazin-1(2H)-one prepared by a novel route. *J. Organomet. Chem.* **690**, 4557–4563
37. Wu, J.Z., Ye, B.H., Wang, L., Ji, L.N., Zhou, J.Y., Li, R.H., and Zhou, Z.Y. (1997) Bis(2,2'-bipyridine)ruthenium(II) complexes with imidazo[4,5-f][1,10]-phenanthroline or 2-phenylimidazo[4,5-f][1,10]-phenanthroline. *J. Chem. Soc., Dalton Trans.* **8**, 1395–1402
38. Liu, Y.C., Yang, Z.Y., Du, J., Yao, X.J., Lei, R.X., Zheng, X.D., Liu, J.N., Hu, H.S., and Li, H. (2008) Study on the interactions of kaempferol and quercetin

- with intravenous immunoglobulin by fluorescence quenching, Fourier transformation infrared spectroscopy and circular dichroism spectroscopy. *Chem. Pharm. Bul.* **56**, 443–451
39. Liu, Y.C., Yang, Z.Y., Du, J., Yao, X.J., Lei, R.X., Zheng, X.D., Liu, J.N., Hu, H.S., and Li, H. (2008) Interaction of curcumin with intravenous immunoglobulin: A fluorescence quenching and Fourier transformation infrared spectroscopy study. *Immunobiology* **213**, 651–661
 40. Bagatolli, L.A., Kivatinitz, S.C., and Fidelio, G.D. (1996) Interaction of small ligands with human serum albumin IIIA subdomain. How to determine the affinity constant using an easy steady state fluorescent method. *J. Pharm. Sci.* **85**, 1131–1132
 41. Yang, M.M., Yang, P., and Zhang, L.W. (1994) Study on interaction of caffeic acid series medicine and albumin by fluorescence method. *Chin. Sci. Bull.* **9**, 31–36
 42. Li, Z.L., Chen, J.H., Zhang, K.C., Li, M.L., and Yu, R.Q. (1991) Fluorescent study on the primary screening for nonplatinum type of Schiff-base antitumor complexes. *Science in China Series B: Chemistry (in Chinese)* **11**, 1193–1200
 43. Baldini, M., Belicchi-Ferrari, M., Bisceglie, F., Pelosi, G., Pinelli, S., and Tarasconi, P. (2003) Cu(II) Complexes with heterocyclic substituted thiosemicarbazones: the case of 5-formyluracil. Synthesis, characterization, X-ray structures, DNA interaction studies, and biological activity. *Inorg. Chem.* **42**, 2049–2055
 44. Ueda, J.-I., Saito, N., Shimazu, Y., and Ozawa, T. (1996) A comparison of scavenging abilities of antioxidants against hydroxyl radicals. *Arch. Biochem. Biophys.* **333**, 377–384
 45. Xing, R., Yu, H., Liu, S., Zhang, W., Zhang, Q., Li, Z., and Li, P. (2005) Antioxidant activity of differently regioselective chitosan sulfates in vitro. *Bioorg. Med. Chem.* **13**, 1387–1392
 46. Chiang, S.Y., Welch, J., Rauscher, F.J., and Beerman, T.A. (1994) Effects of minor groove binding drugs on the interaction of TATA box binding protein and TFIIA with DNA. *Biochemistry* **33**, 7033–7040
 47. Woynarowski, J.M., Mchugh, M., Sigmund, R.D., and Beerman, T.A. (1989) Modulation of topoisomerase II catalytic activity by DNA minor groove binding agents distamycin, Hoechst 33258 and 4',6-diamidine-2-phenylindole. *Mol. Pharmacol.* **35**, 177–182
 48. Chen, A.Y., Yu, C., Gatto, B., and Liu, L.F. (1993) DNA minor groove-binding ligands: a different class of mammalian DNA topoisomerase I inhibitors. *Proc. Natl Acad. Sci. USA* **90**, 8131–8135